Journal of Thermal Analysis and Calorimetry (2023) 148:12891–12905
https://doi.org/10.1007/s10973-023-12554-x

Efficiency of dodecafluoro-2-methylpentan-3-one microemulsion to inhibit thermal runaway in lithium-ion batteries

Yifan Liu[1] · Chongye Chang[1] · Shuhong Li[1] · Jianqi Zhang[1] · Shuai Yuan[1] · Kuo Wang[1] · Xinming Qian[1] · Chi-Min Shu[2]

Received: 4 February 2023 / Accepted: 2 September 2023 / Published online: 10 October 2023

Abstract

Under abusive conditions, lithium-ion battery (LIB) are prone to thermal runaway (TR), which can result in fire and explosion, even toxic. A water-in-oil dodecafluoro-2-methylpentan-3-one ($C_6F_{12}O$) microemulsion was created in this study by emulsifying $C_6F_{12}O$ as the oil phase with a fluorocarbon surfactant, sodium perfluorooctanoate, and a co-surfactant, perfluorobutanol, and encapsulating the aqueous phase. In this paper, the combustion characteristics of 100% SOC LIB and the fire extinguishing experiments of various inhibitors such as microemulsions were carried out; the flame suppression effect, cooling effect and suppression of TR gas production effect of different extinguishing agents were explored; the synergistic suppression mechanism of $C_6F_{12}O$ microemulsions on LIB fires was revealed. The experimental results show that $C_6F_{12}O$ microemulsions can quickly and effectively extinguish LIB flames after release, and their fire extinguishing time is short, which can effectively reduce the generation of high temperature battery fumes and prevent battery re-ignition without short circuit risk. The microemulsion PM1 (61.2% $C_6F_{12}O$, 26.5% water, and the rest emulsifiers) was the most effective: compared with $C_6F_{12}O$ and water, the cooling efficiency was enhanced by 156% and 28%, respectively, and the degree of TR inhibition was enhanced by 18.5% and 24.0%; and the release of cell gas production during inhibition was reduced.

Keywords Fire extinguishing effect · Lithium-ion battery · Microemulsion · Thermal runaway gas · Water immersion

Introduction

Due to their notable attributes such as high energy density, extended cycle periods, elevated voltage levels, and absence of memory effect, Lithium-ion batteries (LIBs) find extensive application in several domains including electric vehicles, electrochemical energy storage systems, and ordinary consumer use [1, 2]. Nevertheless, LIBs are susceptible to thermal runaway (TR) when exposed to abusive circumstances, including excessive charging, overheating, short circuiting, and mechanical impacts [3–8], resulting in smoke, combustion, explosion, and even toxic release, endangering human life and property safety. Extensive study has been conducted on the thermal dangers and safety aspects of lithium-ion batteries (LIBs) in order to effectively mitigate the concerns that must be addressed within the safety framework of the energy storage industry. During the thermal runaway (TR) process, a range of exothermic reactions take place within lithium-ion batteries (LIBs), resulting in an elevation of battery temperature and facilitating more exothermic reactions [7, 9–12]. Furthermore, the process produces huge amounts of flammable and toxic gases, such as H_2, CO, HF, NO_X, and SO_2 [13–15]. An enormous amount of gas build up inside the cell, causing the rupture disk to open. An enormous amount of gas are then ejected from the rupture disk and ignited at high temperatures, resulting in fires and, in extreme cases, explosions in enclosed spaces.

As a result, to reduce the risks of TR in LIBs, different machine learning methods have been successfully used in battery thermal management systems [16]. Researchers have focused their attention on the LIBs fire extinguishing agents, and numerous experiments have been conducted.

✉ Xinming Qian
qsemon@bit.edu.cn

✉ Chi-Min Shu
shucm@yuntech.edu.tw

[1] State Key Laboratory of Explosion Science and Technology, Beijing Institute of Technology, Beijing 100081, China

[2] Department of Safety, Health, and Environmental Engineering, National Yunlin University of Science and Technology, Yunlin 64002, Taiwan, ROC

Water, as an alternative to halon extinguishing agents, does not cause ozone depletion and is absolutely green, non-hazardous, and sustainable [17–20]. Egelhaaf et al. [21] investigated the efficacy of water, an aqueous solution containing the additive F-500, and an aqueous solution containing a geling agent in suppressing LIBs fires. They discovered that water was effective against LIBs fires and that the additive could reduce the amount of water needed to extinguish the fire. Yuan et al. [22] experimentally verified that a 3% F-500 solution is up to three times more effective in cooling LIBs fires than a pure fine water mist. Xu et al. [23] compared and analyzed the suppression effect of three extinguishing agents (CO_2, HFC-227ea, and fine water mist) on LIBs fires, and the results revealed that CO_2 and HFC-227ea could not completely suppress LIBs fires, but fine water mist could. However, Zhang et al. [24] pointed out that when the fine water mist spraying stopped, there was no prominent difference in the cooling rate of the battery; the cooling effect increased with the amount of water, and the water mist did not forestall the propagation of TR, but only delayed it. Furthermore, because of the low contact efficiency, the actual water required to cool the battery is saliently greater than the theoretical water. According to Liu et al. [25], using fine water mist before the critical temperature has a sound cooling impact on the battery and can help prevent TR. However, once the critical temperature has been reached, there is no way to stop the battery from experiencing TR. In recent years, novel halon substitutes have gained popularity for LIB fires due to their strong chemical inhibition, superior insulation, and sound environmental performance. Zhao et al. [26] compared the fire suppression properties of four fire extinguishing agents (fine water mist, $C_6F_{12}O$, ABC, and BC ultra-fine dry powder) and discovered that fine water mist was more effective at cooling, $C_6F_{12}O$ was effective at reducing CO, and the vapor could persist in the air for a long time and put out LIBs fires. Although the cooling effect is limited and LIBs may re-ignite, Liu et al. [27] showed that there is an optimum dose of $C_6F_{12}O$ to put out LIBs fires in a short amount of time. In an experiment, Wang et al. [28] showed that HFC-227ea can extinguish fires in individual cells or small battery packs. However, even after the fire has been put out, the battery's violent reaction is still going on, and flammable gases are constantly being ejected, which could cause the fire to re-ignite. It is possible for the battery to relight. To compare the fire extinguishing and cooling effects of three gaseous fire extinguishing agents—$C_6F_{12}O$, HFC-227ea, and carbon dioxide—in synergistic application with fine water mist on 243Ah large size $LiFePO_4$ cells, Zhang et al. [29] combined gaseous fire extinguishing agents with fine water mist. Compared to single extinguishing agents with the same release mechanism and release time, the results demonstrate that the synergistic application of gaseous fire extinguishing agents with fine water mist provides better fire extinguishing and cooling effects.

In summary, the existing body of research on fire extinguishing agents for lithium-ion batteries can be categorized into two main groups. One course focuses on the study of water mist and water mist extinguishing agents with additives. These agents are essentially water-based extinguishing agents that possess a notable attribute of effectively cooling lithium-ion batteries through continuous application. The fire extinguishing and cooling capacity of additives can be enhanced by modifying their characteristics. However, it is important to note that the inadequate insulation of the extinguishing agent has the potential to induce a short circuit in lithium-ion battery systems, leading to a secondary fire. Consequently, the high conductivity of water can be considered a critical limitation in this context. Another category is defined by the utilization of perfluorohexanone, heptafluoropropane, and other halon alternatives as the primary gaseous agent for fire suppression. This category is distinguished by its potent chemical inhibition properties, enabling rapid extinguishment of battery fires. Additionally, the agent exhibits prolonged persistence in the air, allowing for continuous action. However, it is important to note that this category's cooling effect is insufficient, resulting in inadequate suppression of rekindling.

The TR reaction of LIBs in a heated, pressurised tank device was studied by Koch et al. [30], who also examined, measured, and determined the emission gases' affecting components. The results showed that energy density and battery capacity were significant determinants of the number of emissions, with CO_2, CO, H_2, C_2H_4, CH_4, C_2H_6, and C_3H_6 accounting for over 99% of the emitted gases, with CO_2, CO, and H_2 being the predominant ones. The principal emitted gas components for various battery types were found, along with the concentrations, by Yuan et al. [31], who researched the gases released from LIBs with various chemical compositions. Peng et al. [14] employed a toxic gas model to quantitatively assess the overall toxicity of the released gas and discovered that lithium iron phosphate batteries with a higher state of charge (SOC) had a greater fire risk in terms of toxic gas concentrations. In their study of the combustion and explosion risks associated with the TR in lithium cobaltate batteries, Somandepalli et al. [32] experimentally investigated and characterized the gas composition, explosion limits, and other indicators. They discovered that the main flammable gas components were CO, H_2, and hydrocarbons, and they established the lower explosion limit (LEL) and upper explosion limit (UEL) of the released gases in various charge states. Zhang et al. [33] investigated the toxicity of the gas released during the TR of ternary LIBs. They used effective dose fraction and effective concentration models to assess the gas toxicity and discovered

that the effect of HF was the most prominent and that the system's gas toxicity increased following water spraying. To determine the toxicity of the HF and SO_2 gases released from small-capacity lithium iron phosphate batteries and to forecast the toxicity of the entire lithium-ion module, Lecocq et al. [34] conducted combustion tests on the batteries. [15], Larsson et al. [35, 36] performed fire tests to quantify the toxic fluoride gases released from different types of LIBs. They discovered that the fine release of water mist increased the rate of HF production and that the lower the charge state, the more HF was produced.

Numerous studies have been conducted to examine the concentration and composition of gases emitted by TR. These investigations have involved diverse chemical components within LIB systems. Present evaluations of gas hazards primarily center on the inherent risks of combustion, explosion, and toxicity associated with the batteries themselves. To yet, there has been a lack of scholarly examination and assessment about the impact of extinguishing chemicals on the emission of gases from thermal runaway batteries.

This paper aims to investigate the fire combustion characteristics of lithium iron phosphate batteries under thermal runaway conditions. To achieve this, a battery thermal runaway and fire extinguishing platform will be established. The study will involve conducting thermal runaway combustion inhibition experiments using a perfluorohexanone microemulsion. The inhibitory effects of perfluorohexanone and fine water mist as extinguishing agents will be compared, analyzing their respective flame inhibition effects, cooling effects, and gas release. The findings of this research will provide theoretical support and guidance for selecting appropriate extinguishing media and agents for lithium iron phosphate batteries, as well as contribute to the development of safety standards for batteries.

Experiments

Battery

A 50 Ah LIB with a positive electrode material of $LiFePO_4$ was selected for this study, consisting of electrode material, electrolyte, separator, aluminum case, safety vent, and current collector. The battery had a nominal voltage of 3.2 V and a prismatic shape with dimensions of 148 mm (L) × 28 mm (D) × 116 (H) mm. Before testing, the battery was discharged to a cut-off voltage of 2.5 V by constant current (10A, i.e., 0.2C) and then charged to a 100% state of charge (SOC) by 10A constant current, at which point the full charge cut-off current was 1A.

Experimental setup

The experimental setup, as shown in Fig. 1, consisted primarily of an explosion-proof box, a fire extinguishing system, a battery module box, a battery heating system, a temperature data acquisition system, a ventilation device, a gas collection device, a gas analyser, and a camera.

The explosion-proof box measured 1 m × 0.7 m × 1.8 m and had explosion-proof glass on the front, allowing the external camera to record the entire experimental process. A fire extinguishing agent storage tank, water pump,

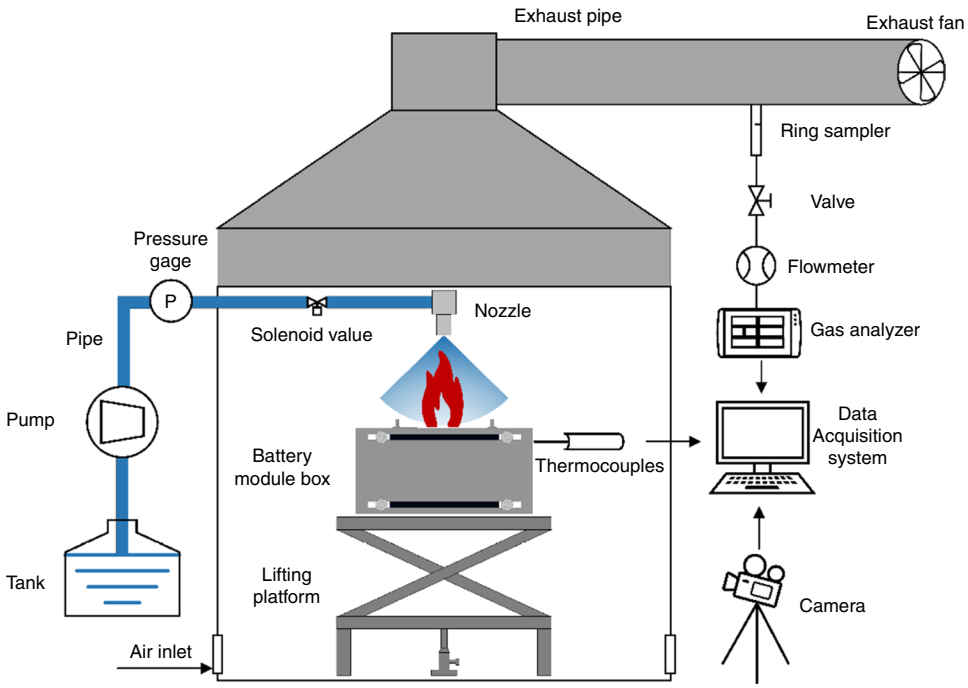

Fig. 1 Diagram of the experimental setup

pressure gauge, solenoid valve, water pipe, and atomizing nozzle were the main components of the fire extinguishing system. A 500 W electric heating plate, an electric heating unit, and a temperature control box were included in the battery heating system. The temperature acquisition system consisted of a K-type thermocouple and a real-time display instrument with a 1 time/s acquisition frequency. The gas analyser had a 1 time/s acquisition frequency and a range of 1 ~ 20,000 ppm. As shown in Fig. 2(a), to prevent heat loss into the air, the batteries were placed in parallel in the battery module box, close to a heating plate of the same size as the batteries, clamped with two steel plates separated by a heat insulation plate. The heating plate was heated with an electric heating device until the battery experiences TR and was ignited with a manual electric igniter. During the test, 10 K-type thermocouples were distributed around the LIB to detect the battery's surface, flame, and ambient temperature; the thermocouple distribution is shown in Figs. 2(b) and (c). K1 monitored the temperature at the center of the heating plate, K2–K4 were distributed diagonally along the long surface of the battery, and the average temperature of K2–K4 measured the temperature of the long surface of the battery, K5 monitored the temperature of the battery's side surfaces, K6 monitored the temperature of the positive terminal of the battery, and K7 surveiled the temperature of the flame 20 cm above the battery. To exhaust the fumes produced by the cell's TR, an explosion-proof fan with a power of 0.18 kW and a gas pipe with a volume flow rate of 622 m^3/h were used. During the experiment, a gas analyser was used to measure the concentrations of CO, CO_2 and H_2 in real-time.

The tank was filled with various fire extinguishing solutions, and the agent was released through an atomizing nozzle with a working pressure of 5.5 MPa and a flow rate of 1.62 L/min. The nozzle was 30 cm from the top of the battery, resulting in a fine water mist atomisation angle of 60°, which was sufficient to cover the entire battery range. When the LIB emitted gas, a pointed flame ignited the smoke, resulting in a stable flame. When one of the thermocouple temperatures T_1, T_2, or T_3 exceeded 150 °C and the temperature rise rate exceeded 1 °C s^{-1}, the pump was activated, allowing the extinguishing agent to be released.

Fire extinguishing agent preparation

In essence, $C_6F_{12}O$ is insoluble in water because it is a perfluorocarbon compound. In this study, sodium perfluorooctanoate surfactant was used as the emulsifier and perfluorobutanol as the co-emulsifier, with a mass ratio of 2:1. To make the oil phase solution, a certain amount of the compounded surfactant was thoroughly mixed with the oil phase of $C_6F_{12}O$ and stirred for 10 min with a constant temperature magnetic stirrer until homogeneous. Then, drop by drop, added deionised water to the solution of $C_6F_{12}O$ dissolved in surfactant, each drop after adding a certain amount of water, ultrasonic treatment instrument for 3 min, deionised water after all drops were added and stood for a period of time to obtain $C_6F_{12}O$ and water of the water-in-oil microemulsion. Conductivity was one of the most important parameters affecting water-based extinguishing agents that caused short circuits outside the battery system [37]; therefore, determining its conductivity, and characterizing the insulating properties of water-based extinguishing agents, was critical. At room temperature, the conductivity of microemulsions was measured using a conductivity tester (model DDSJ-308F, measuring range 0.000–1000 mS/cm, minimum resolution 0.001 μ S/cm, temperature range – 5.0–110.0 °C).

There are a variety of component ratios in the manufactured microemulsions due to the limitations of the emulsifier and the characteristics of the oil phase $C_6F_{12}O$, and water accounts for up to 26.5% of the total. The

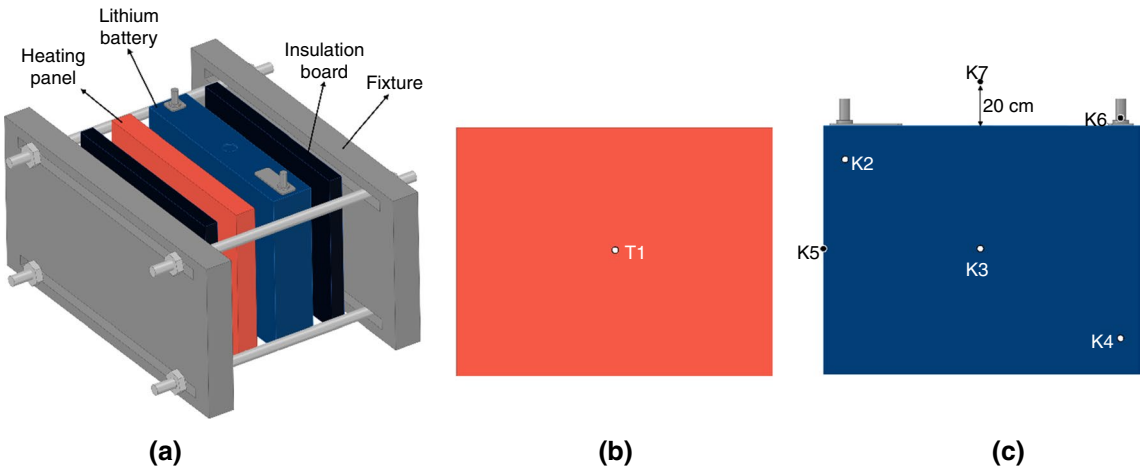

Fig. 2 Battery module box and thermocouple distribution: **a** overall view, **b** heating plate surface, and **c** cell surface

Table 1 Parameters of $C_6F_{12}O$ microemulsions

Fire extinguishing agent	Percentage of $C_6F_{12}O$ / %	Percentage of water / %	Electrical conductivity / μ S/cm
PM1	61.2	26.5	3.92 ± 0.15
PM2	66.7	20	3.89 ± 0.20
PM3	73.2	12.2	3.75 ± 0.16

Table 2 Experimental working conditions

Case	Extinguishing agent	Agent dosage / kg	Pressure / MPa	Electrical conductivity / μ s/cm
#1	No agent	–	–	–
#2	Tap water	1	5.5	380 ± 2.40
#3	$C_6F_{12}O$	1	5.5	0
#4	PM1	1	5.5	3.92 ± 0.15
#5	PM2	1	5.5	3.89 ± 0.20
#6	PM3	1	5.5	3.75 ± 0.16

parameters of the $C_6F_{12}O$ microemulsion extinguishing agent used for the experiments are listed in Table 1. Three different ratios of microemulsions, PM1, PM2, and PM3, were prepared according to the different ratios of $C_6F_{12}O$ and water, and water and $C_6F_{12}O$ were used as control groups to suppress the battery TR and flame.

Experimental working conditions

The suppression effects of $C_6F_{12}O$, water, and three ratios of microemulsions on battery fire and fire characteristic parameters were compared with battery combustion without fire extinguishing agent, to explore the performance of $C_6F_{12}O$ microemulsions in suppressing TR and fire extinguishing in the LIB. The experimental conditions are listed in Table 2.

Results and discussion

Combustion behavior of the battery

The battery combustion process is shown in Fig. 3, and the temperature change of the battery surface is shown in Fig. 4.

From Figs. 3 and 4, the thermal runaway and combustion process of lithium iron phosphate batteries can be divided into four stages: (I) warming and exhaust stage; (II) stable combustion stage; (III) intense combustion stage; (IV) flame extinguishing stage.

In stage I, with the continuous heating of the electric heating plate, the battery heat gradually accumulates, the temperature of thermocouple K1 directly connected to the heating plate T_1 rises rapidly, and the temperature of the thermocouple connected to the battery is also increasing, as T_5 and T_6 are closer to the heating plate, their temperature rise rate is greater than that of T_2, T_3 and T_4 on the other long surface of the battery. A series of reactions begin to occur inside the battery at this stage. The solid electrolyte interface film (SEI) will start to decompose first at around 90–120°C, and the reaction is shown in Eq. (1). And the electrolyte inside the battery, such as ethylene carbonate (EC), dimethyl carbonate (DMC), diethyl carbonate (DEC) and other organic solvents react with Li and other organic solvents in the negative electrode to produce a large amount of gases such as C_2H_4, as shown in Eqs. (2–4). This leads to the accumulation of gas and heat inside the cell, and the surface deforms and expands due to the increase in internal pressure, at which point no thermal runaway occurs.

$$(CH_2OCO_2Li)_2 \longrightarrow Li_2CO_3 + C_2H_4 + CO_2 + 1/2O_2 \quad (1)$$

$$2Li + C_3H_4O_3(EC) \longrightarrow Li_2CO_3 + C_2H_4 \quad (2)$$

$$2Li + C_3H_6O_3(DMC) \longrightarrow Li_2CO_3 + C_2H_6 \quad (3)$$

$$2Li + C_5H_{10}O_3(DEC) \longrightarrow Li_2CO_3 + C_4H_{10} \quad (4)$$

In stage II, the internal pressure reaches the threshold, the safety valve opens, ejecting a large amount of gas and

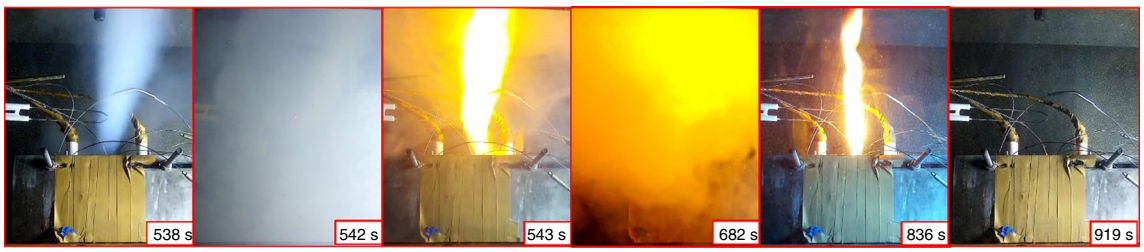

Fig. 3 Battery combustion without extinguishing agent

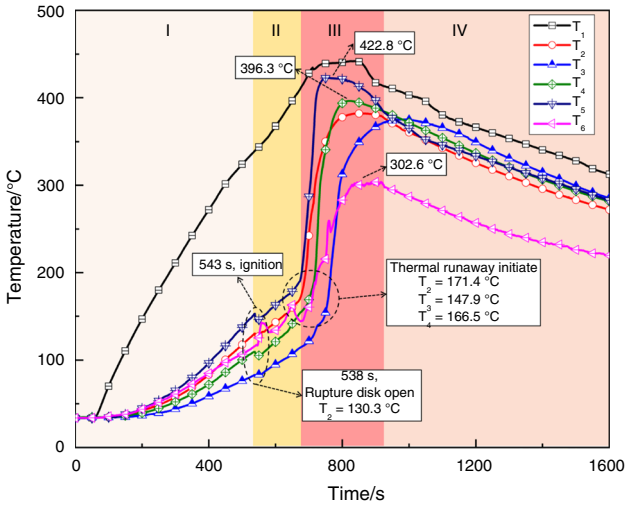

Fig. 4 Temperature change without extinguishing agent

smoke; high-temperature gas products are ejected into the environment, taking away some of the heat, making the temperature of each thermocouple on the surface of the battery have different degrees of decline. Safety valve open lithium iron phosphate battery will not occur after spontaneous combustion, you need to manually open the electric igniter. At 543 s, the gas is ignited by the electric ignition spark, a jet fire occurs, the flame first strong and then weakened and then tends to stabilize. Affected by the flame heat radiation, the positive thermocouple temperature T_6 fluctuates relatively large, while the other thermocouple temperature is less affected. At this stage, with the accumulation of internal heat, the decomposition reaction of cathode material $LiFePO_4$ occurs, the electrolyte $LiPF_6$ reacts to generate HF and other toxic gases, EC and DMC with the generated oxygen to generate a large amount of CO_2, as shown in Eqs. (5–8).

$$2LiFePO_4 \longrightarrow FeP_2O_7 + 1/2O_2 \tag{5}$$

$$LiPF_6 + H_2O \longrightarrow LiF + POF_3 + 2HF \tag{6}$$

$$5/2O_2 + C_3H_4O_3(EC) \longrightarrow 3CO_2 + 2H_2O \tag{7}$$

$$3O_2 + C_3H_6O_3(DMC) \longrightarrow 3CO_2 + 3H_2O \tag{8}$$

In phase III, the cell burns violently, with the flame becoming brighter and lighter in color, and burns violently for about 50 s. The cell surface temperature rises sharply, with the temperature rise rate at each measurement point rising from less than 0.5 °C s^{-1} previously to more than 1 °C s^{-1}. This change occurs first at T_5, followed by T_2, T_3, and T_4, because TR is first triggered at the heated surface, and then spreads along the cell thickness direction and then propagates to the whole cell. The interval between T_5, where thermal runaway occurs first, and T_3, where thermal runaway occurs last, is the propagation time of thermal runaway inside the cell, Δt, which is 72 s. And it can be assumed that thermal runaway has occurred and shows signs of propagation when the temperature on the side of the cell exceeds 150 °C and the temperature rise rate is greater than 1 °C s^{-1}. It can be obtained that it is better to release the extinguishing agent before the thermal runaway occurs at T_2, T_3 and T_4, i.e. before the thermal runaway of the whole battery. The surface temperature of the battery reaches the peak temperature within 200 s. The temperature change trend of T_2, T_3 and T_4 is more or less the same, and finally rises to 370–400 °C, and the peak temperature of T_5 is 422.8 °C. At this stage, most of the internal materials are involved in the combustion reaction, and the electrolyte undergoes decomposition reaction, as in Eq. (9).

$$C_2H_5OCOOC_2H_5 + PF_5 \longrightarrow C_2H_5OCOOPF_4 + HF + C_2H_4 \tag{9}$$

In stage IV, the battery continued to burn steadily for about 100 s without using extinguishing agent before the flame was extinguished and only some smoke was emitted. The internal chemical reaction stops, and no further thermal runaway occurs within 1 h. At this point, the thermal runaway is considered to be over.

Inhibition effect of different fire extinguishing agents

Different fire extinguishing agents were used to suppress the battery flame and compare their fire extinguishing effects. Figure 5 shows the suppression process of thermal runaway and combustion of $LiFePO_4$ battery without fire extinguishing agent, $C_6F_{12}O$, water and three ratios of microemulsion. The fire extinguishing effect of different extinguishing agents on lithium iron phosphate fires is shown in Table 3.

After the release of $C_6F_{12}O$, the flame of $LiFePO_4$ was extinguished within 1 s. This is mainly due to the rapid vaporization of $C_6F_{12}O$ released into the combustion zone, which reacted with the combustion radicals and quickly interrupted the chain reaction and terminated the combustion process. However, after the flame is extinguished, some smoke and aerosols will still be produced, stop releasing for electrical ignition, the lithium-ion battery did not re-ignite, mainly because the vaporized $C_6F_{12}O$ gas continues to remain in the closed space, a short period of time did not evaporate, at this time reached the inert concentration, so it will not re-ignite. Under the action of pure fine water mist, the battery flame was pushed around and below the impact force and then extinguished. After stopping the release of fine water mist, the battery still produces high-pressure jet gas inside, at this time for electric ignition,

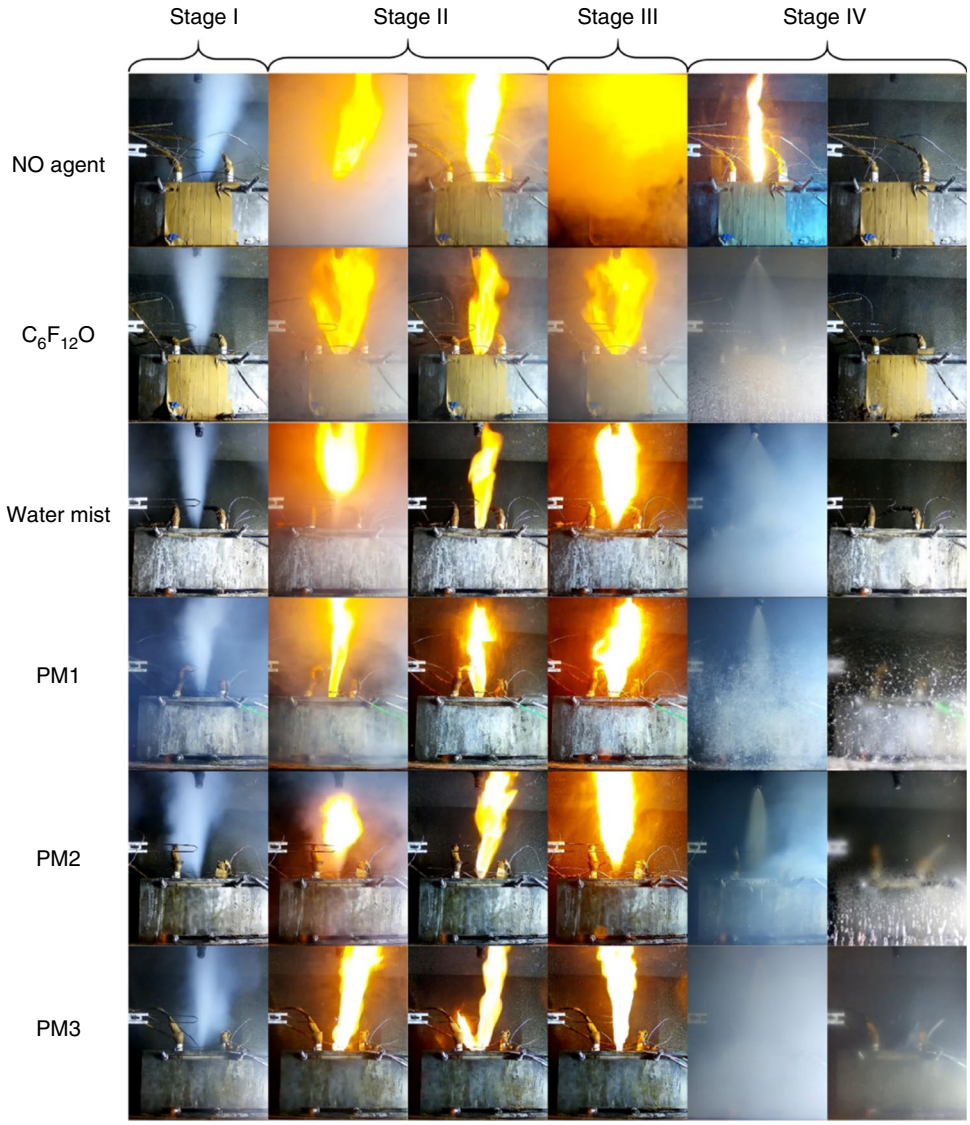

Fig. 5 Battery combustion under different extinguishing agents

Table 3 Effect of different agents on thermal runaway combustion of battery

Agent	Inhibitory effect				
	Extinguishing time	Battery status after the fire is extinguished	Reignition condition	Residue	Short-circuit condition
$C_6F_{12}O$	< 1 s	Emit a lot of smoke	No	Nothing	No
Water	< 5 s	High-pressure gas injection	Yes	Bulk water	Yes
PM1	< 1 s	Emit a small amount of smoke	No	Partial foam	No
PM2	< 1 s	Emit a small amount of smoke	No	Partial foam	No
PM3	< 1 s	Emit a small amount of smoke	No	Small foam	No

three experiments, one electric ignition short circuit, two re-ignition occurred, but the flame did not continue to burn under the jet gas, lasted a few tens of seconds and then stopped, the bottom of the battery with liquid water residue. After the release of the three ratios of microemulsions, as the dispersed phase is $C_6F_{12}O$, contact with the combustion zone, the oil phase $C_6F_{12}O$ quickly vaporized, and the battery flame was similarly extinguished within 1 s. However, unlike the pure fine water mist, after the release of PM1, PM2 and PM3 stopped, the battery only produced a small

amount of smoke and there was no high-pressure gas jet, at which time the ignition was carried out and no re-ignition occurred. Also the microemulsion release produces a foam as shown in Fig. 6, which is produced by the low interfacial tension of the fluorocarbon surfactant, which increases the duration of the cooling and suppression effect. Microemulsions increase the cooling effect of water can inhibit the combustion of $C_6F_{12}O$, in addition, the decomposition of $C_6F_{12}O$ in microemulsions can enhance the fire extinguishing effect of water.

Cooling efficiency analysis

The temperature variation of the LIB indicates the suppression effect of the extinguishing agent on the thermal runaway of the LIB and is also considered as an important parameter to evaluate the effectiveness of the extinguishing agent. Figure 7 gives the changes of battery temperature under the action of different extinguishing agents. It can be seen that the battery surface temperature decreases with the release of the extinguishing agent, but the battery temperature continues to increase after the extinguishing agent stops releasing and even during the release. This is mainly due to the LIB thermal runaway process is irreversible, the extinguishing agent can only reduce the intensity of thermal runaway, but can not stop the thermal runaway process. Under the action of the fire extinguishing agent, the temperature changes at each part of the LIB surface are different. T_{234} is not in direct contact with the fire extinguishing agent, its decline is small in the process of fire extinguishing agent release, the fire extinguishing agent release occurs after the rise. T_5 and T_6 are in direct contact with the fire extinguishing agent in the process of fire extinguishing agent release, the magnitude of change is larger. Among them, T_6 is subject to the impact of the fire extinguishing agent, which occurs with greater fluctuations. In which the water release process, the LIB surface temperature drop is more effective. This is mainly because the specific heat capacity of water and the latent heat of vaporization is relatively large, in the fine water mist contact with the surface of the LIB, warming and then vaporization to take away a large amount of heat, and fine water mist surface tension is small, the spray of small water droplets can reach the long surface of the LIB through the gap, thus reducing the surface temperature. Although the chemical inhibition of $C_6F_{12}O$ can extinguish the flame of the LIB, the large amount of gas mixture generated after the open fire above the LIB is extinguished is ejected through the safety valve to form a high-temperature smoke shower, thus inhibiting $C_6F_{12}O$ from entering the negative combustion zone of the LIB where chemical inhibition is required. And because $C_6F_{12}O$ has a low boiling point and vaporizes rapidly upon contact with the LIB, it does not easily reach the long surface of the LIB, so the temperature of the LIB does not drop significantly under the action of $C_6F_{12}O$. However, after the release of the three microemulsions, the synergistic effect of $C_6F_{12}O$ and water significantly reduced the degree of thermal runaway of the LIB and lowered the peak LIB temperature.

Fig. 6 Foam produced after release of the microemulsion inhibitor

The rebound of T_{234} temperature after the release of extinguishing agent indicates the intensity of thermal runaway, and is expressed by Eqs. (10)–(11). The changes of T_5 and T_6 highlight the transient cooling ability of extinguishing agent on the LIB surface, and the change of battery surface temperature T_5 is more typical, and is expressed by Eq. (12).

$$\Delta T_a = T^0_{234,peak} - T^i_{234,peak} \tag{10}$$

$$\Delta T_b = T^i_{234,peak} - T^i_{234,end} \tag{11}$$

$$\Delta T_c = T^i_{5,start} - T^i_{5,end} \tag{12}$$

$T^0_{234,peak}$ represents the peak temperature of T_{234} without extinguishing agent action; $T^i_{234,peak}$ represents the peak temperature of T_{234} with extinguishing agent action; $T^i_{234,end}$ represents the instantaneous temperature of T_{234} after the end of extinguishing agent release; $T^i_{5,start}$ represents the instantaneous temperature of T_5 before extinguishing agent release; $T^i_{5,end}$ represents the instantaneous temperature of T_5 after the end of extinguishing agent release.

The ΔT_a, ΔT_b, and ΔT_c under the different extinguishing agents are shown in Fig. 8. The maximum ΔT_a under the action of PM1 indicates that PM1 has the best overall inhibition effect, which is 156% higher compared with $C_6F_{12}O$ and 28% higher compared with water. Taking the degree of peak temperature reduction of T_{234} as the reference basis, the inhibition effect is PM1 > PM2 > water > PM3 > $C_6F_{12}O$. This indicates that when the water content in the compound microemulsion reaches a certain percentage, the combined effect of $C_6F_{12}O$ and water is better for cooling the cell surface than their individual effects. This is due to the fact that after the compound solution is ejected, the $C_6F_{12}O$ component can quickly extinguish the flame and the water

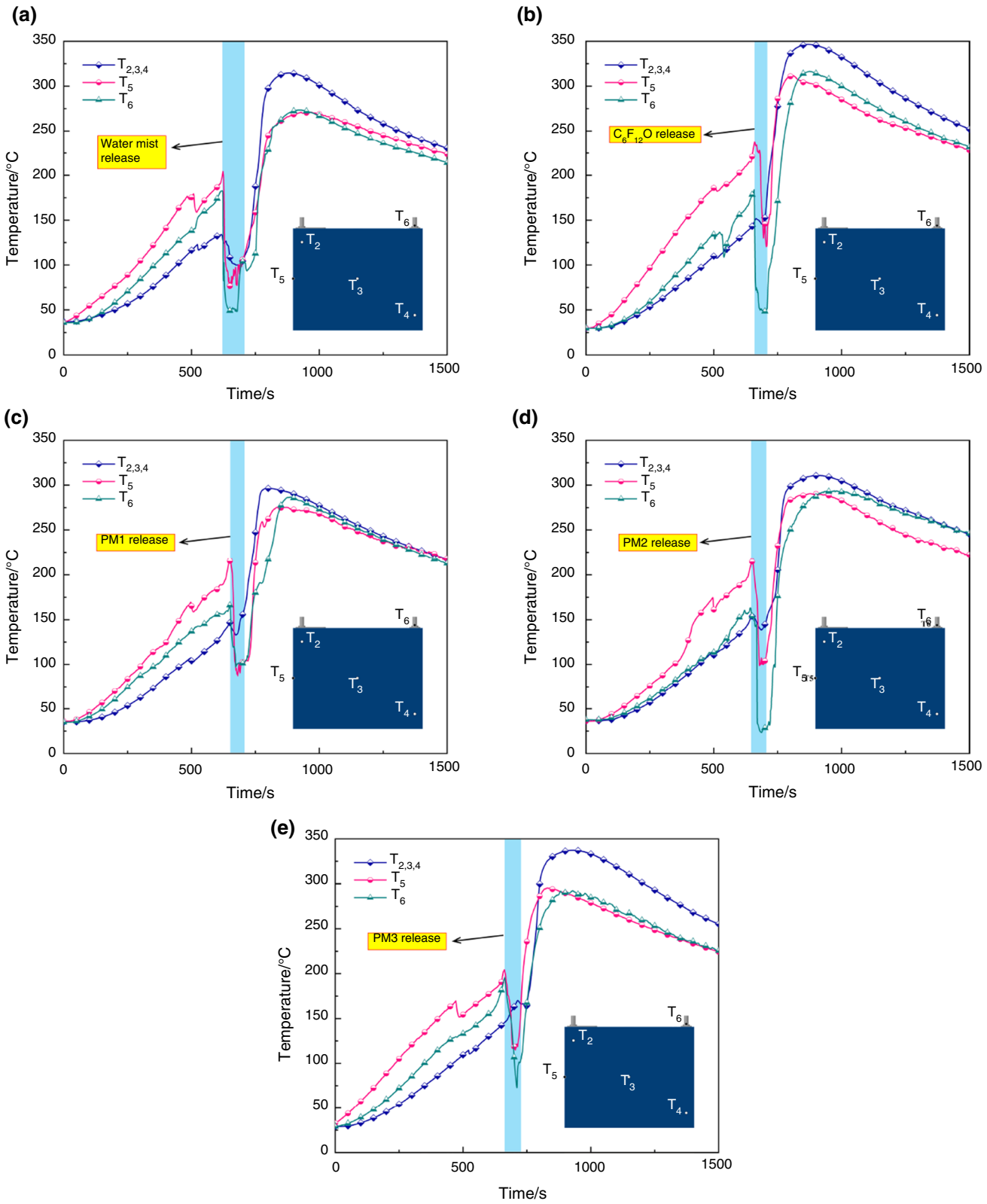

Fig. 7 LIB surface temperature changes under different extinguishing agents

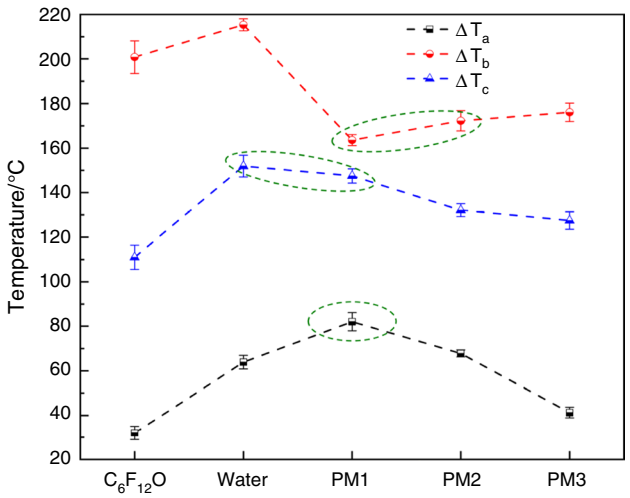

Fig. 8 The ΔT_a, ΔT_b and ΔT_c under different extinguishing agents

component can inhibit the high temperature plume released from the LIB, making it easier for the $C_6F_{12}O$ component to contact the LIB and inhibit the internal thermal runaway chain reaction, while both components can better cool down the LIB.

In addition, the ΔT_b of PM1 was 163.63°C, which was 18.5% lower compared to $C_6F_{12}O$ and 24.0% lower compared to water. Using the degree of thermal runaway intensity of the LIB after the end release of the extinguishing agent as the reference basis, the inhibition effect was PM1 > PM2 > PM3 > $C_6F_{12}O$ > water in the order of good to bad. The peak temperature under the action of water is smaller than that under the action of $C_6F_{12}O$, but ΔT_b is larger instead, which indicates that the inhibiting effect of $C_6F_{12}O$ on the thermal runaway reaction inside the battery is much larger than that of water. The mass of $C_6F_{12}O$ component in PM1, PM2 and PM3 increases in order, but ΔT_b increases in order, which indicates that the inhibiting efficiency of $C_6F_{12}O$ is higher under the synergistic action of water.

Unlike ΔT_a and ΔT_b, the heat absorbed by the fire extinguishing medium on the side of the cell during the release of the extinguishing agent by convective cooling is much larger than the heat transferred from the inside of the cell to the side. ΔT_c is water, PM1, PM2, PM3, and $C_6F_{12}O$ in descending order, and the content of water gradually decreases, and this change result also confirms that the transient cooling effect of water is better than that of $C_6F_{12}O$. In addition, it can be seen that there is a substantial reduction in the peak cell side temperature with different extinguishing agents. The ΔT_c of PM1 is 147.5 ± 3.22°C, a 34.9% decrease compared to the unreleased extinguishing agent.

Figure 9 depicts the rate of temperature change of T_5 during the extinguishing agent's release and post-release warming phase. Figure 9 shows that the maximum temperature drop rate of T_5 under the influence of PM1 is − 25.7 °C s^{-1}, which was similar to the rate under the influence of water and greater than the rate under the influence of PM2 and PM3. It was evident that case 2 had two peaks that resulted from the battery's severe TR and that the $C_6F_{12}O$ release process did not entirely stop the battery's temperature rise. The graph also showed that during this phase, the T_5 temperature fluctuated above and below 0, with periods of rising and falling during the T_5 temperature rise rate after the release of water and PM1. This was because after the extinguishing agent ceased discharging, $C_6F_{12}O$ would evaporate, and water would still be present on the battery's surface, causing the surface temperature to fluctuate due to the battery's internal exotherm and the cooling of the external residual water droplets until all the water droplets evaporated and the temperature rise rate commenced to turn positive [27]. This manifested that the release of water slowed the rise in cell temperature, and the duration of temperature swings on the surface demonstrated the extinguishing agent's slowing impact. The retarding effect of PM1 was greater than 20 s, but the effect was essentially nonexistent following the release of $C_6F_{12}O$.

Gas release

The response of CO, CO_2 and H_2 concentrations under different suppression of fire extinguishing agents during the LIB combustion is shown in Fig. 10. It can be seen that after the safety valve is opened, the concentration of H_2 increases rapidly at first, followed by the concentration of CO. After igniting the jet, H_2 and CO are partly ignited and the concentration decreases to some extent, but the gas is still continuously ejected from inside. H_2 reaches up to 8300 ppm without extinguishing agent, CO concentration fluctuates around 600 ppm, while the concentration of CO_2 starts to increase rapidly. After the internal material of the cell is fully burned and ejected, the concentration of H_2 and CO starts to decrease, and the concentration of CO_2 also decreases rapidly until it reaches the normal concentration.

The total release of CO, CO_2 and H_2 under different extinguishing agent inhibition is shown in Table 4. Although the extinguishing agent chemically and physically inhibits the internal reactions and reduces the gas production, the extinguishing agent also inhibits the open flame, which leads to incomplete combustion of electrolyte and electrode materials, so the concentration of CO does not decrease much in the presence of the extinguishing agent compared with the effect without the extinguishing agent. On the contrary, the release of CO in the presence of $C_6F_{12}O$ is much larger than that without fire extinguishing agent, which is due to the fact that at high flame temperatures of 700–800 °C, $C_6F_{12}O$ and free radicals generate CO through pyrolysis and bonding, while $C_6F_{12}O$ undergoes decomposition reactions at high temperatures to generate CO. The $C_6F_{12}O$ content of PM1,

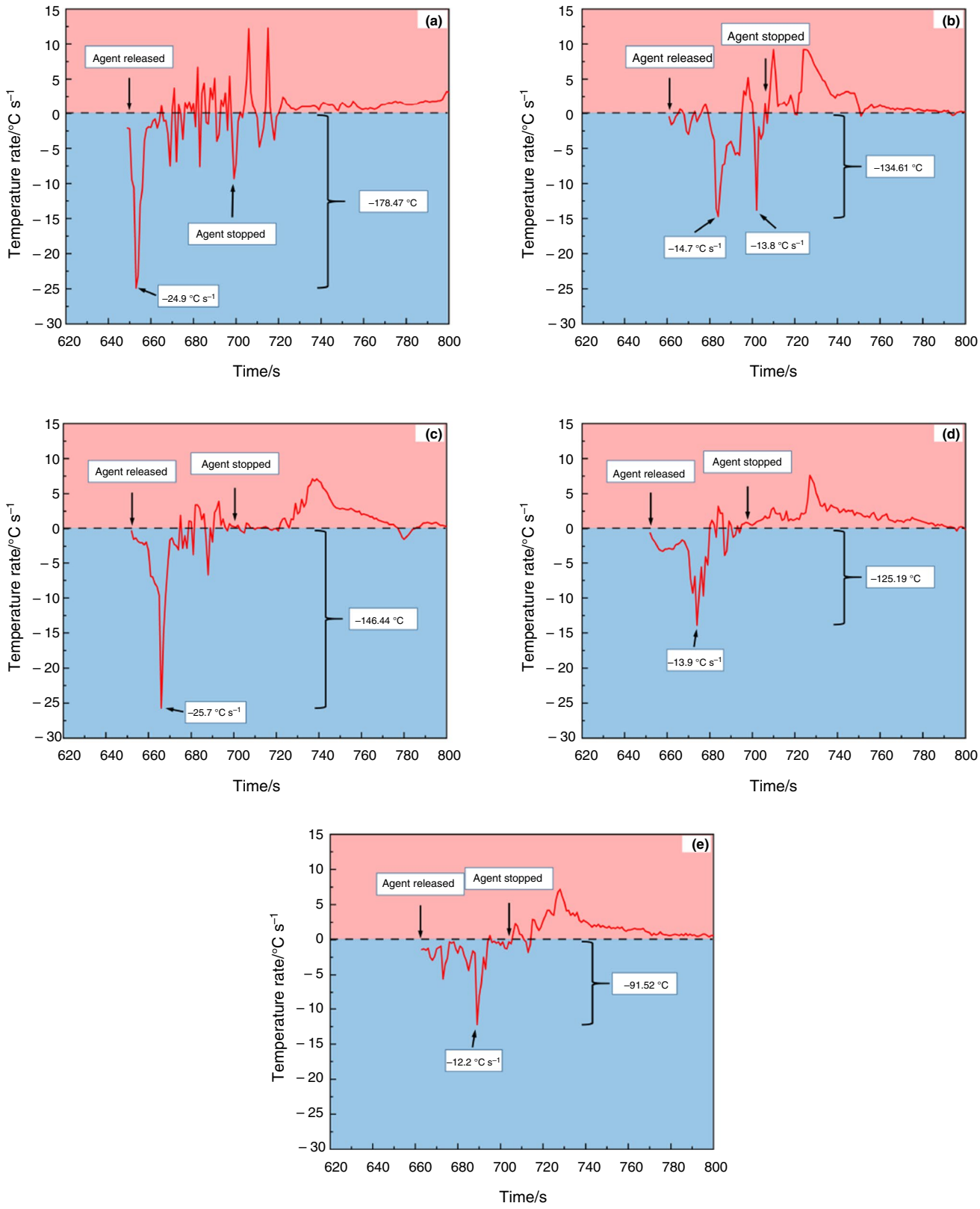

Fig. 9 Rate of temperature change of T_5 during the release and post-release warming phase of the extinguishing agent **a** $C_6F_{12}O$, **b** water, **c** PM1, **d** PM2, and **e** PM3

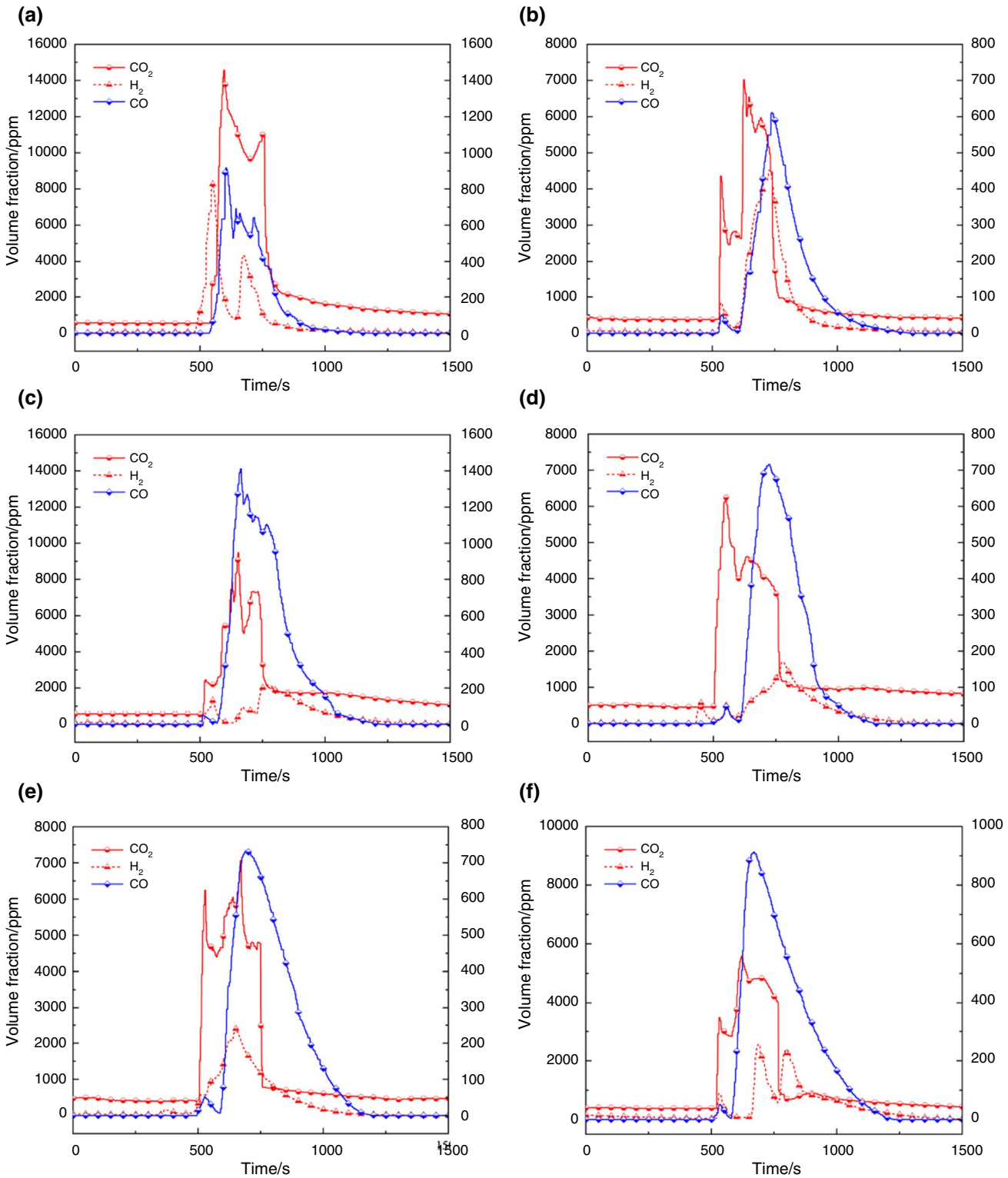

Fig. 10 Gas concentration change curve under different extinguishing agent suppression

PM2, and PM3 is reduced, and at the same time the cooling effect are better and all produce less CO than under $C_6F_{12}O$ release, but all still have a portion of $C_6F_{12}O$, so all have higher CO concentrations than under water spray. The CO release under PM1 action is 1.50×10^5 ppm, which is 50.8% lower compared to $C_6F_{12}O$.

Table 4 Total release of TR gas from LIB under different fire extinguishing agents

Gas volume	Agent					
	No agent	Water	$C_6F_{12}O$	PM1	PM2	PM3
CO / ppm	1.45×10^5	1.15×10^5	3.06×10^5	1.51×10^5	1.92×10^5	2.28×10^5
CO_2 / ppm	2.82×10^6	1.24×10^6	1.84×10^6	1.45×10^6	1.49×10^6	1.29×10^6
H_2/ ppm	9.55×10^5	7.41×10^5	6.16×10^5	4.23×10^5	5.33×10^5	5.94×10^5

It can be seen from the CO_2 release and real-time concentration that the maximum CO2 concentration and total release under different extinguishing agents are much smaller than those under no extinguishing agent release. Since CO_2 mainly originates from the decomposition at the solid electrolyte interface, oxidation of electrolyte and electrode, and complete combustion of alkane products, the reduction of CO_2 release indicates that $C_6F_{12}O$, water, PM1, PM2, and PM3 all inhibit the thermal runaway of the LIB and reduce or even block the decomposition and reduction reactions inside the LIB. The CO_2 release under the action of PM1 is 1.45×10^6 ppm which is 21.4% lower compared with $C_6F_{12}O$. It is also further demonstrated that $C_6F_{12}O$ generates additional CO, which increases the asphyxiating toxicity of the system.

The extinguishing agent does not produce additional H_2, so it all originates from the thermal runaway products of the LIB. Compared with the case without extinguishing agent, the H_2 release was reduced by 35.5% and 22.4% with $C_6F_{12}O$ and water, respectively. Both $C_6F_{12}O$ and water inhibited thermal runaway to some extent, and the effect of $C_6F_{12}O$ was better than that of water. However, the H_2 release was reduced by 55.6%, 44.2% and 37.8% under the inhibitory effect of PM1, PM2 and PM3, respectively, and the inhibitory effect was better than that of $C_6F_{12}O$ and water.

Synergistic inhibition mechanism

The synergistic inhibition mechanism of $C_6F_{12}O$ microemulsion on TR of LIB can be represented by Fig. 11, taking PM1 as an example.

At the beginning of the fire extinguishing agent release phase, the vaporization and heat absorption of $C_6F_{12}O$ and water reduces the flame temperature, and then $C_6F_{12}O$ absorbs a large amount of flame heat and decomposes, and the fluorinated radicals generated participate in the chain reaction of combustion, consuming a large number of combustion radicals and destroying the chain reaction of flame combustion, which greatly reduces the flame propagation speed and flame temperature.

The reduction of combustion intensity prompted the fine water mist to reach the LIB surface, which has a high heat capacity and a high specific surface area and can quickly absorb heat and vaporize, cooling the LIB surface rapidly, while the final battery flame was extinguished under the

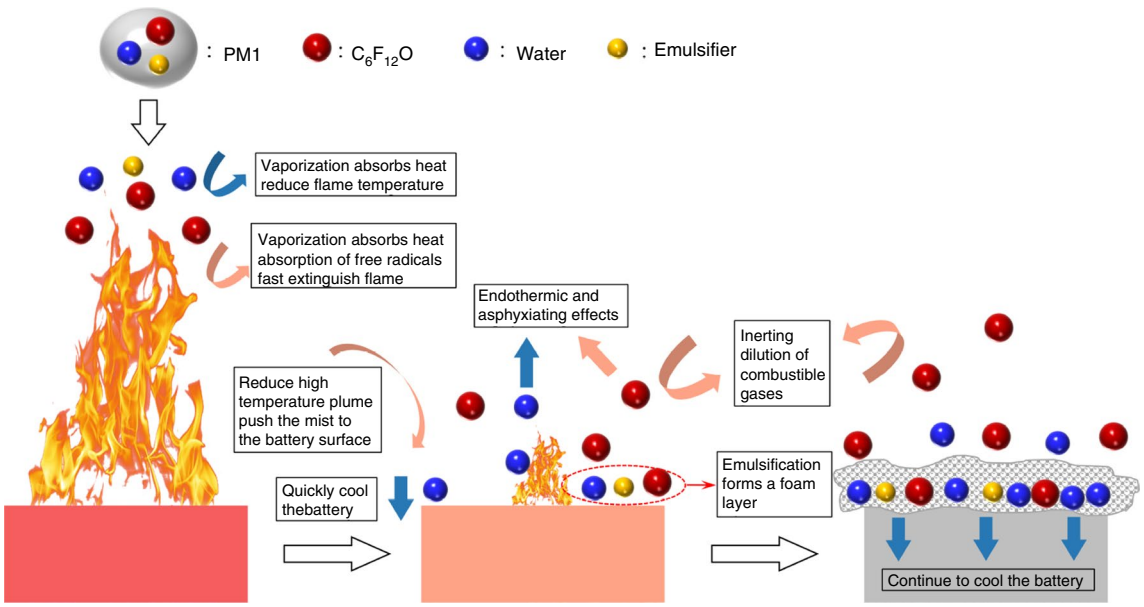

Fig. 11 Mechanism of microemulsion inhibiting TR of LIB

physical heat absorption and asphyxiation effect of $C_6F_{12}O$ and water.

The gas produced by the vaporization of $C_6F_{12}O$ dilutes and inert the combustible gas near the LIB, preventing the battery from re-igniting. And $C_6F_{12}O$ and water are emulsified by the action of emulsifiers, i.e. surfactants and co-surfactants, to produce a foam layer covering the surface of the LIB for continuous cooling and cooling.

In summary, the physical heat absorption effect of $C_6F_{12}O$, the chemical inhibition effect of consuming free radicals, the efficient cooling effect of fine water mist and the continuous cooling effect of microemulsion foam layer synergistically complement each other to extinguish the LIB flame, cool the LIB temperature, prevent the LIB from re-ignition, and effectively suppress the LIB fire.

Conclusions

In summary, this paper analyzes the TR combustion characteristics of $LiFePO_4$ battery, and uses $C_6F_{12}O$, water, and three homemade $C_6F_{12}O$ microemulsions for suppression, with the following main conclusions:

(1) 100% SOC $LiFePO_4$ battery requires an external ignition source to start a fire after the safety valve is opened, and the total combustion time from fire to flame extinguishment is 376s; the peak temperature of the LIB surface can reach 422.8°C; the propagation time of TR inside the LIB is 72 s.

(2) The fire suppression effect of $C_6F_{12}O$ microemulsion on LIB is better than that of $C_6F_{12}O$ and water: The fire extinguishing time is shorter; the generation of high temperature battery smoke is effectively reduced, which reduces the intensity of TR of the battery; foam and $C_6F_{12}O$ gas are produced after release, which effectively prevents the battery from re-ignition; the insulation performance is excellent.

(3) PM1 microemulsion (61.2% of $C_6F_{12}O$, 26.5% of water, the rest is emulsifier) has the best cooling and cooling effect and inhibits the degree of TR: The peak temperature of the LIB surface is reduced by 82.03 °C, and the cooling efficiency is enhanced by 156% and 28% compared with $C_6F_{12}O$ and water, respectively; the degree of TR of the LIB is reduced, and the LIB temperature rises back after releasing the extinguishing agent 163.63°C, which enhanced the degree of inhibition by 18.5% and 24.0% compared with C6F12O and water; the instantaneous cooling effect reduced the peak side temperature of the LIB by 147.5 °C, or 34.9%.

(4) CO is released during perfluorocaprolactone inhibition, while $C_6F_{12}O$ microemulsion can reduce the release of CO and substantially reduce the release of H_2 and CO_2 during thermal runaway. Under the effect of PM1, the release of CO and CO_2 were reduced by 50.8% and 21.4%, respectively, compared with $C_6F_{12}O$, and the release of H_2 was reduced by 55.6% compared with no fire suppressant.

Acknowledgements This work was supported by the National Key Research and Development Program of China [grant number 2017YFC0804700].

Author contributions YL: Conceptualization, Investigation, Validation, Formal analysis, Writing-original draft; CC: Validation, Data Curation, Investigation; SL: Investigation, Data Curation; JZ: Investigation; SY: Investigation; KW: Investigation; MY: Investigation; XQ: Conceptualization, Methodology, Project administration, Supervision; QX: Writing-review and editing, Supervision.

Declarations

Competing interest The authors declare that they have no known competing financial interests or personal relationships that could have appeared to influence the work reported in this paper.

References

1. Poizot P, Dolhem F. Clean energy new deal for a sustainable world: from non-CO_2 generating energy sources to greener electrochemical storage devices. Energy Environ Sci. 2011;4:2003–19.
2. Ni S, Tan S, An Q, Mai L. Three dimensional porous frameworks for lithium dendrite suppression. J Energy Chem. 2020;44:73–89.
3. Ohsaki T, Kishi T, Kuboki T, Takami N, Shimura N, Sato Y, Sekino M, Satoh A. Overcharge reaction of lithium-ion batteries. J Power Sources. 2005;146:97–100.
4. Ye J, Chen H, Wang Q, Huang P, Sun J, Lo S. Thermal behavior and failure mechanism of lithium ion cells during overcharge under adiabatic conditions. Appl Energy. 2016;182:464–74.
5. Kitoh K, Nemoto H. 100 Wh large size Li-ion batteries and safety tests. J Power Sour. 1999;81:887–90.
6. Wu T, Chen H, Wang Q, Sun J. Comparison analysis on the thermal runaway of lithium-ion battery under two heating modes. J Hazard Mater. 2018;344:733–41.
7. Wang Q, Ping P, Zhao X, Chu G, Sun J, Chen C. Thermal runaway caused fire and explosion of lithium ion battery. J Power Sour. 2012;208:210–24.
8. Ji H, Chung Y-H, Pan X-H, Hua M, Shu C-M, Zhang L-J. Study of lithium–ion battery module's external short circuit under different temperatures. J Therm Anal Calorim. 2021;144:1065–72.
9. Wang Y-W, Shu C-M. Energy generation mechanisms for a Li-ion cell in case of thermal explosion: a review. J Energy Storage. 2022;55:105501.
10. Liu P, Li Y, Mao B, Chen M, Huang Z, Wang Q. Experimental study on thermal runaway and fire behaviors of large format lithium iron phosphate battery. Appl Therm Eng. 2021;192:116949.
11. Kim SW, Park SG, Lee EJ. Assessment of the explosion risk during lithium-ion battery fires. J Loss Prev Process Ind. 2022;80:104851.
12. Wang K, Cao Y, Yang Y, Wang Z, Ouyang D. Exploring fluorinated electrolyte for high-voltage and high-safety Li-ion cells with $Li(Ni0.8Mn0.1Co0.1)O_2$ cathode. Int J Energy Res. 2022;46:24243–53.

13. Ribière P, Grugeon S, Morcrette M, Boyanov S, Laruelle S, Marlair G. Investigation on the fire-induced hazards of Li-ion battery cells by fire calorimetry. Energy Environ Sci. 2012;5:5271–80.
14. Peng Y, Yang L, Ju X, Liao B, Ye K, Li L, Cao B, Ni Y. A comprehensive investigation on the thermal and toxic hazards of large format lithium-ion batteries with $LiFePO_4$ cathode. J Hazard Mater. 2020;381:120916.
15. Larsson F, Andersson P, Blomqvist P, Mellander B-E. Toxic fluoride gas emissions from lithium-ion battery fires. Sci Rep. 2017;7:1–13.
16. Can A, Selimefendigil F, Öztop HF. A review on soft computing and nanofluid applications for battery thermal management. J Energy Storage. 2022;1(53):105214.
17. Zhou Y, Bu R, Gong J, Zhang X, Fan C, Wang X. Assessment of a clean and efficient fire-extinguishing technique: continuous and cycling discharge water mist system. J Cleaner Prod. 2018;182:682–93.
18. Zhou Y, Bu R, Zhang X, Fan C, Gong J. Performance evaluation of water mist fire suppression: a clean and sustainable fire-fighting technique in mechanically-ventilated place. J Cleaner Prod. 2019;209:1319–31.
19. Cui Y, Liu J. Research progress of water mist fire extinguishing technology and its application in battery fires. Process Saf Environ Prot. 2021;149:559–74.
20. Xu J, Duan Q, Zhang L, Liu Y, Sun J, Wang Q. The enhanced cooling effect of water mist with additives on inhibiting lithium ion battery thermal runaway. J Loss Prev Process Ind. 2022;77:104784.
21. Egelhaaf M, Kress D, Wolpert D, Lange T, Justen R, Wilstermann H. Fire fighting of Li-Ion traction batteries. SAE Int J Altern Powertrains. 2013;2:37–48.
22. Yuan S, Chang C, Zhang J, Liu Y, Qian X. Experimental investigation of a micelle encapsulator F-500 on suppressing lithium ion phosphate batteries fire and rapid cooling. J Loss Prev Process Ind. 2022;79:104816.
23. Xu J, Guo P, Duan Q, Yu X, Zhang L, Liu Y, Wang Q. Experimental study of the effectiveness of three kinds of extinguishing agents on suppressing lithium-ion battery fires. Appl Therm Eng. 2020;171:115076.
24. Zhang L, Duan Q, Liu Y, Xu J, Sun J, Xiao H, Wang Q. Experimental investigation of water spray on suppressing lithium-ion battery fires. Appl Therm Eng. 2021;120:103117.
25. Liu T, Liu Y, Wang X, Kong X, Li G. Cooling control of thermally-induced thermal runaway in 18,650 lithium ion battery with water mist. Energy Convers Manage. 2019;199:111969.
26. Zhao J, Xue F, Fu Y, Cheng Y, Yang H, Lu S. A comparative study on the thermal runaway inhibition of 18650 lithium-ion batteries by different fire extinguishing agents. iScience. 2021;24:102854.
27. Liu Y, Duan Q, Xu J, Chen H, Lu W, Wang Q. Experimental study on the efficiency of dodecafluoro-2-methylpentan-3-one on suppressing lithium-ion battery fires. RSC Adv. 2018;8:42223–32.
28. Wang Q, Shao G, Duan Q, Chen M, Li Y, Wu K, Liu B, Peng P, Sun J. The efficiency of heptafluoropropane fire extinguishing agent on suppressing the lithium titanate battery fire. Fire Technol. 2016;52:387–96.
29. Zhang L, Li Y, Duan Q, Chen M, Xu J, Zhao C, Sun J, Wang Q. Experimental study on the synergistic effect of gas extinguishing agents and water mist on suppressing lithium-ion battery fires. J Energy Storage. 2020;32:101801.
30. Koch S, Fill A, Birke KP. Comprehensive gas analysis on large scale automotive lithium-ion cells in thermal runaway. J Power Sour. 2018;398:106–12.
31. Yuan L, Dubaniewicz T, Zlochower I, Thomas R, Rayyan N. Experimental study on thermal runaway and vented gases of lithium-ion cells. Process Saf Environ Prot. 2020;144:186–92.
32. Somandepalli V, Marr K, Horn Q. Quantification of combustion hazards of thermal runaway failures in lithium-ion batteries. SAE Int J Altern Powertrains. 2014;3:98–104.
33. Zhang L, Duan Q, Meng X, Jin K, Xu J, Sun J, Wang Q. Experimental investigation on intermittent spray cooling and toxic hazards of lithium-ion battery thermal runaway. Energy Convers Manag. 2022;252:115091.
34. Lecocq A, Eshetu GG, Grugeon S, Martin N, Laruelle S, Marlair G. Scenario-based prediction of Li-ion batteries fire-induced toxicity. J Power Sour. 2016;316:197–206.
35. Larsson F, Andersson P, Blomqvist P, Lorén A, Mellander B-E. Characteristics of lithium-ion batteries during fire tests. J Power Sour. 2014;271:414–20.
36. Larsson F, Bertilsson S, Furlani M, Albinsson I, Mellander B-E. Gas explosions and thermal runaways during external heating abuse of commercial lithium-ion graphite-$LiCoO_2$ cells at different levels of ageing. J Power Sour. 2018;373:220–31.
37. Zhou Y, Bai J, Wang Z, Wang J, Bai W. Inhibition of thermal runaway in lithium-ion batteries by fine water mist containing a low-conductivity compound additive. J Cleaner Prod. 2022;340:130841.